Available online at www.sciencedirect.com

ScienceDirect

Procedia Structural Integrity 52 (2024) 543–550

Structural Integrity Procedia

www.elsevier.com/locate/procedia

Fracture, Damage and Structural Health Monitoring

Recovery of Interlaminar Tensile Stresses in Curved Laminates Subject to Biaxial Flexure: The Case of an Elastically Induced Curvature Purposely Misaligned with the Principal Directions of Initial Curvature

Lorenzo Marchignoli[a], Enrico Bertocchi[a], Matteo Giacopini[a], Valerio Mangeruga[a]

[a]*University of Modena and Reggio Emilia, Engineering Department "Enzo Ferrari", via Vivarelli 10, 41125 Modena (MO), Italy*

Abstract

Many literature contributions deal with the evaluation at FE post-processing stage of the interlaminar normal stress distribution in moderately thick single or doubly curved laminates subject to flexure, based on through-the-thickness equilibrium relations. Most of the contributions, however, discuss test cases in which the principal directions of the load-induced elastic curvatures are aligned with the principal directions of the initial curvature; this condition is not general. In the present work, a simple post-processing methodology for the recovery of the interlaminar tensile stress is presented.
The procedure retrieves the Interlaminar Tensile Stresses (ILTS) distribution in a doubly curved laminate modelled through common wise quadrilateral shell Finite Elements and is based on customary FE sub-model which inputs are the displacements and rotation calculated on the shell structure. At the moment the sub-model can't retrieves Interlaminar Shear Stresses but can be further enhanced to do it.
In this paper the methodology is successfully applied to an open thin walled profile in torsion test case, in which the principal directions of elastic curvature are strongly misaligned with the principal directions of initial curvature.

Keywords: Stress recovery; Linear Shell Element; Transverse Stresses, Delamination;

1. Introduction

Nowadays, structures made of laminates in composite materials are extensively utilized in motorsport due to their lightweight compared to rigidity and strength. The need to obtain increasingly optimized components leads to the requirement for calculation tools that allow for better prediction of their strength and at the same time be efficient in terms of computational cost.

10.1016/j.prostr.2023.12.054

The present contribution describes a procedure for retrieving the Interlaminar Tensile Stresses (ILTS) distribution in a curved (and possibly doubly-curved) laminate modelled through commonwise four-noded, quadrilateral shell Finite Elements; the procedure is operated at post-processing stage.

ILTS are responsible, along with the Interlaminar Shear Stresses (ILSS), of laminate delamination failures ; albeit the latters are addressed by the shell elements embedded in the customary FE packages, see e.g. (Dassault System 2006; MSC Software Corporation 2013 a), the ILTS may be appreciated only by resorting to a 3d solid discretization of the laminate, an approach, this, which becomes less and less computationally viable while moving from local submodels to whole structures.

In order to create a procedure with reduced computational time, compared to 3d solid mesh approach, in literature many authors have proposed a stress recovery method based on the a posteriori integration of the through-the-thickness laminate equilibrium equation.

Rolfes, Rohwer, and their colleagues (Rolfes et al. 1997, 1998, 2000) achieved with their FSDT continuous interlaminar stresses by integrating the equations of local equilibrium through the thickness and proposed an element‐wise formulation called the Extended‐2D method.

A stress recovery method based on the a posteriori integration of the through-the-thickness laminate equilibrium equation is presented in (Roos et al. 2007 a) based on the analytical formulation developed in (Huang et al. 1992), however such stress recovery method neglects the contribution to the ILTS of the in-plane shear strain component, an assumption, this, which holds when the principal directions of geometric (initial) curvature are aligned with either the principal direction of orthotropy for the various laminae, or with the principal directions of elastic curvature. Those conditions — albeit only minimally violated in most of the test cases proposed in literature, see e.g.(Kress et al. 2005; Roos et al. 2007 a)— do not hold in general, moreover (Pagano 1970) developed exact solutions for multilayered plates and showed that warping of cross-sections exist. A complete stress recovery method proposed by (Daniel et al. 2020) gave good results but its computational cost still not be assessed.

In the present contribution, a test case is first proposed in which the geometric curvature is strongly (45°) misaligned with both the principal direction of the elastic curvature, and the principal directions of material orthotropy; also, the geometric and the elastic curvatures are uniform along the specimen surface, a condition, this, which limits the response dependence on mesh size and distortion when patch test compliant shell elements are employed.

Then, a ILTS recovery procedure is applied, which relies on the assembly of a pile stack of customary quadratic (20-noded) hexahedral elements — one each laminate layer, indicatively — within a framework of kinematic constraints which reproduce the nodal motion of the underlying shell element under scrutiny.

The resort to standard elements from the FE solver library is an advantage of the present method since it grants the ready availability of most of the material formulations, and of the customary pre- and post-processing procedures for model definition, and result analysis.

The obtained results are then compared, along with the predictions returned by the method proposed in (Roos et al. 2007 b), with those of a full 3d model.

2. Test Case Description

A simple test has been developed to investigate the possible role of the missing in-plane shear strain component within the (Roos et al. 2007 b) formulation. The aim is to generate an elastic curvature whose principal directions are 45° inclined with respect to the geometric curvature, in order to maximize the angular discrepancy between those direction. Such a condition is typical of an open thin-walled (or moderately thick-walled) “C” shaped circular arc cross section profile subject to torsion. The lamination has been also chosen in order to maximize its unsymmetric nature with respect to the midsurface, and the fiber orientation is chosen in order to be highly unsymmetrical with respect to the principal directions of curvature. The FE test case, depicted in Fig. 1, consists in a single curvature geometry derived as an angular portion of an hollow cylinder with axis along Z direction, whose inner, midsurface and outer radii equate 0.5 mm, 1 mm and 1.5 mm, respectively - thus obtaining a unit thickness to mean radius ratio.

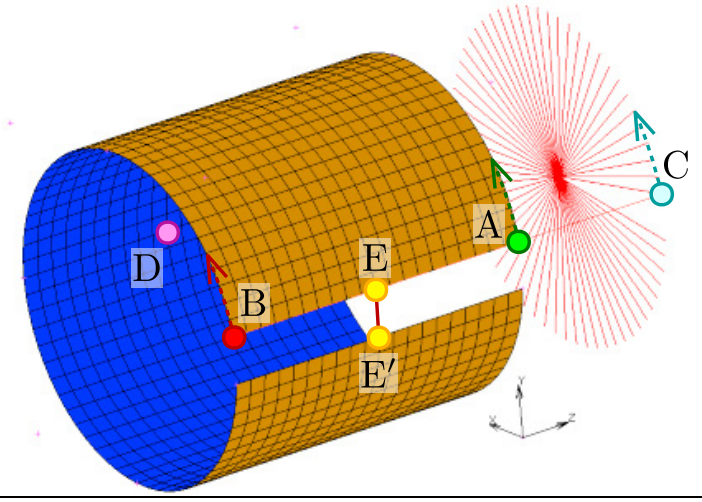

Fig. 1. Details of the domain under investigation.

The midsurface is discretized with a structured quadrilateral mesh counting 60 elements along the circumferential direction — each of which encompasses a 0.1 radians arc, and 20 0.1 mm wide elements along the axial direction; the overall angular extension of 6 radians (≈343.77°) lets the (limited) free edge perturbation at the C profile opening to decay before reaching the central gauge area of the model.

Customary shear deformable (Mindlin type) four noded, bilinear (Taig) quadrilateral shell elements are employed; the elements are identified as "type 75" within the MSC.Marc Element Library, (MSC Software Corporation 2013 b), and similar elements are available in Nastran (CQUAD4) or Abaqus (S4). The proposed procedure may be straightforwardly applied to i) any shell element whose degrees of freedom consists in the full set of nodal translations and rotations, with the possible exception of the drilling rotation, and ii) the pentahedral/hexahedral solid shell elements, for which the nodal rotations may be derived from the top/bottom differential displacements. Most of the available shell elements are hence encompassed, with the notable exception of the Irons semiloof shell element (Irons 1976).

The elements' normals are inward oriented, with a inner shell top surface, and an outer shell bottom surface; material orientation is defined with respect to the axial Z direction, so that a 0° oriented unidirectional ply is characterized by axially oriented fibers.

The laminate is composed by 10 plies with a thickness of 0.1 mm each, the offset is null so that the shell elements and the associated nodes are positioned along the midsurface.

The material for all the plies is a UD CFRP composite whose properties are defined in Table 1.

Table 1. Material properties.

Unidirectional CFRP Properties		
Longitudinal Elastic Modulus	E_1	150 [GPa]
Transverse Elastic Moduli	$E_2 = E_3$	6 [GPa]
Poisson ratios	ν_{12}	0.05 [-]
	ν_{23}	0.3 [-]
	ν_{31}	0.016 [-]
Shear Moduli	G_{12}	6 [GPa]
	$G_{23} = G_{31}$	5 [GPa]

The first - innermost - five plies are oriented at +45° and remaining – outermost - five plies are oriented at 45°. As told before, the laminate is deliberately non symmetric, non-balanced, and designed to exhibit the most general membrane/curvature elastic coupling as described in CLT (Jones, 1999). Details of the laminate material is depicted in Fig. 2

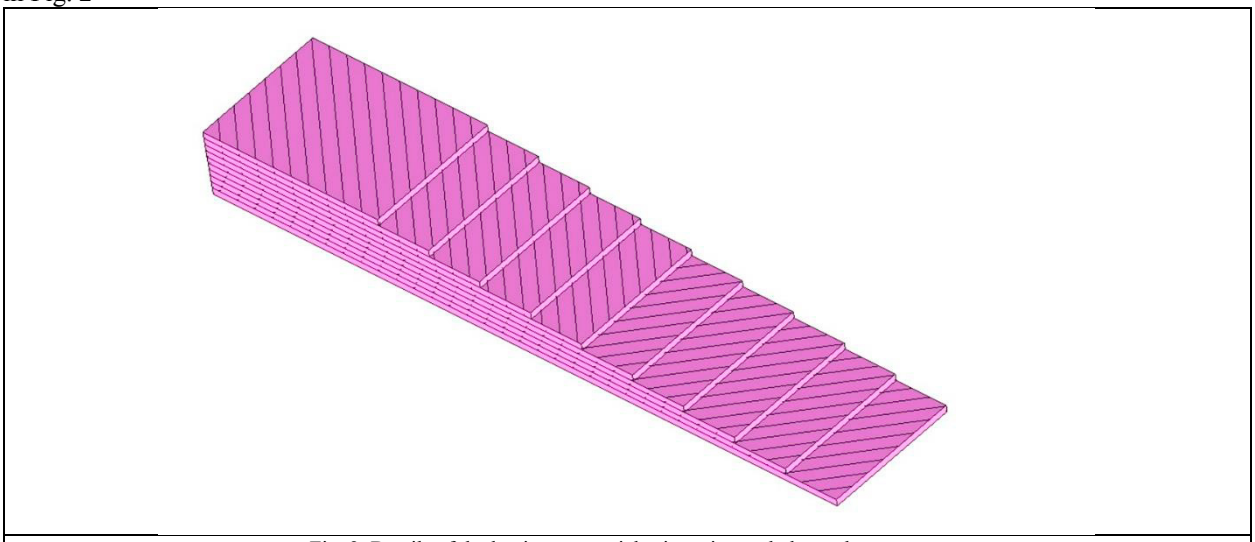

Fig. 2. Details of the laminate material orientation and ply stack sequence.

The two axial extremities of the profile segment are node-wisely kinematically linked in order to enforce a periodic displacement and rotation field, apart from an imposed differential twist rotation; in this way the warping motion predicted by the De Saint Venant torsion is allowed, alongwith any further assessment possibly induced by the lack material of symmetry with respect to the cross sectional plane. Also, the modeled portion is representative of an infinitely long profile subject to twist.

The actual kinematic link implementation consists in a rigid body RBE2 link, which drives the differential twist rotation between the two the modeled profile portion ends, and a set of multi-point constraints (MPC) in which the displacements/rotations of each node (labeled as "A" in Fig. 1) along one profile extremity are tied to the sum of the displacements/rotations of the corresponding nodes at the other end, and at the RBE2 (labeled as "B" and "C", respectively, in Fig. 1).

The RBE2 is conveniently placed next to the mesh, with a centrally located master node; the actual positioning of the RBE2 within the model is unimportant, as unimportant is the location of its master node, if — apart from the imposed twist rotation — a strictly statically determinate set of constraints is employed to suppress the six residual rigid body motions of the discretized profile segment, and hence uniquely position its deformed configuration in space.

With reference to Fig. 1, we employed the following set of imposed displacement conditions: a centrally located (but possibly arbitrary) point D along the profile segment is locked in x,y, and z translations in order to suppress the associated rigid body motions.; equal and opposite y displacements are imposed to the two facing (and shifted in x with respect to D) E, E' nodes through a MPC, in order to suppress the residual rotation around the (D,z) axis; the RBE2 master node D is supported in the x and y directions, in order to suppress the rotations around the (D,x), (D,y) axes. Finally, a unit (1 rad) z rotation is imposed at the RBE2 master node, in order to produce a imposed 0.5 rad/mm twist rate; the obtained results may be freely scaled due to the problem linearity.

By radially extruding the quadrilateral elements of the shell model, a 3d hexahedral solid element model is derived, for comparison. To increase the stress prediction capabilities of this control model, triquadratic, 20 node elements have been employed (element type 21 according to the MSC.Marc Element Library, see (MSC Software Corporation 2013 b)). A single 3d hexahedral layer has been employed for each lamina. The previously defined set of kinematic constraints is applied to this solid element model. The solid model adopted for the comparison is depicted in Fig. 3.

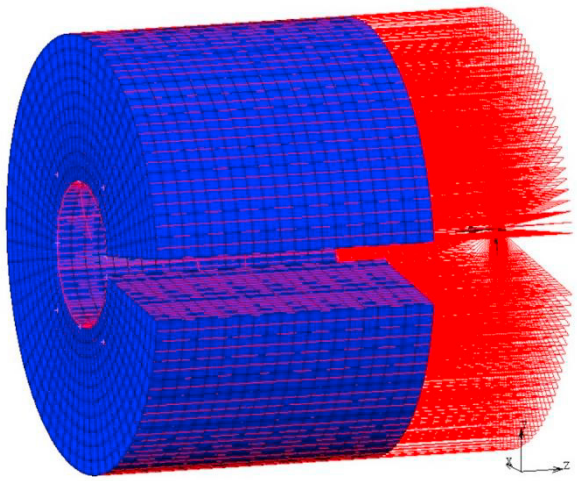

Fig. 3. Fully solid model used for the comparison.

In Fig. 4 below the deformed shapes are reported for both the solid element model and the shell model. This particular test loading condition generates an axial-circumferential mixed elastic curvature, whose principal directions are ±45° inclined with respect to the axial and the circumferential directions, and which is hence not aligned with the principal curvature of the geometry.

Along the shell model, membrane stretching and curvatures are sampled in the neighborhood of the central node D, in order to minimize the influence of free edge perturbations. For the laminate under scrutiny, the nonzero generalized components consist in the mixed axial-circumferential curvature $\kappa_{ac} = -1$, in accordance with the imposed twist rate, open thin-walled profile torsion theory, and an equibiaxial membrane contraction $\varepsilon_a = \varepsilon_c = -0.1149$.

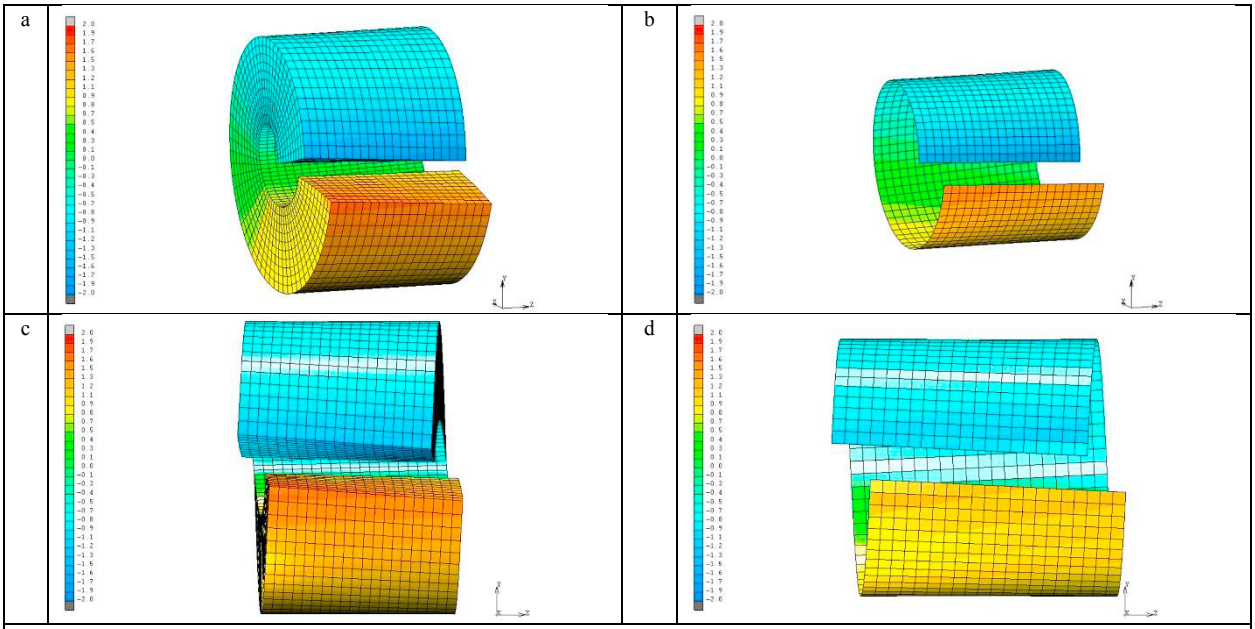

Fig. 4. Comparison of deformation: the 3D solid FE model (a), and the 2D shell FE model (b), with details of the warping effect for the first model (c) and for the second model (d). The contour plot represents the displacement in Z referenced to the global coordinates.

The through-the thickness variation of the notable, nonzero strain components is reported for both the hex20 control model and the quad4 shell model in Fig. 5. Due to the curved nature of the profile wall, the shear strain component γac induced by the elastic curvature significantly deviates from linearity in the control model.

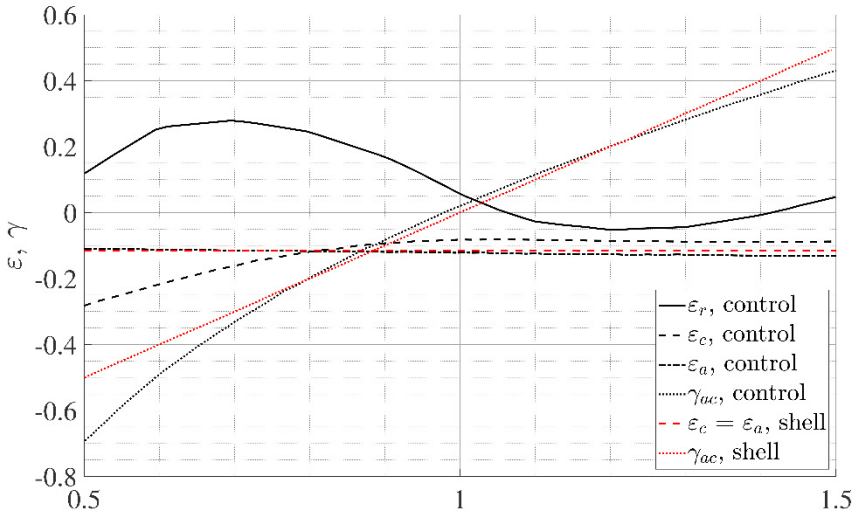

Fig. 5. Through-the-thickness variation of the nonzero strain components in the hex20 control model (black lines) and in the quad4 shell model (red lines); the inner and the outer surfaces correspond to radial positions equal to 0.5 and 1.5 mm, respectively.

The ILTS values returned by the control model are reported in Fig. 6, along with the predictions obtained by applying the reference (Roos et al. 2007 b) procedure; being the proposed test case designed for highlighting the role of the in-plane shear terms, which are neglected by such procedure, its results deviate significantly from the control counterpart.

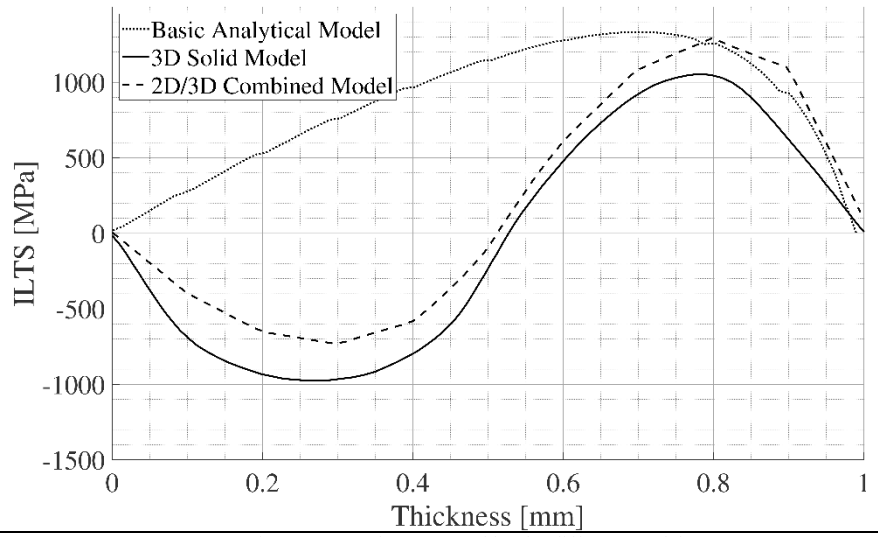

Fig. 6. ILTS values returned by the different models.

3. A Postprocessing Procedure for the ILTS

In order to overcome to the limits of the ref. (Roos et al. 2007 b) formulation, a novel method is proposed, which may be classified as a one-way, uncoupled global/local stress recovery procedure, see (Mao et al. 1991), and which is detailed in the following.

The quadrilateral shell elements of the base model are processed once at time; for each element under scrutiny, a stress recovery submodel is created that represents the associated laminate sector in the form of a through-the-thickness stack of 20-noded hexahedral elements, one (or possibly more) element each layer, as shown in Fig. 7. A single per layer hex20 quadratic element has been employed in the present contribution.

Normal directions are defined at the underlying shell element nodes, whose angular aperture is obtained based on the nominal surface curvatures; those normal directions define the orientation in space of the solid submodel lateral edges, and implicitly introduce curvature-awareness to the submodel response.

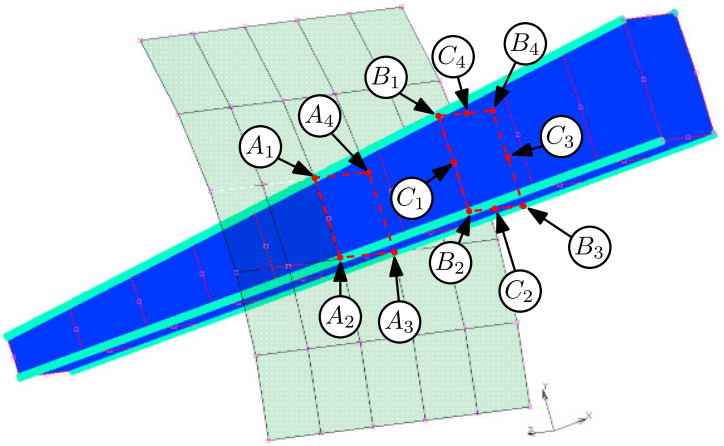

Fig. 7. Details of the stress recovery model developed.

Four RBE2 rigid body kinematic constraints – represented as cyan round bars in Fig. 7 – tie the tangential displacements of the nodes lying along the submodel lateral edges (labelled as B1,B2, etc. in Fig. 7) to the roto-translations of the associated underlying shell element node (labelled as A1, A2 etc. in Fig.7) , as returned by the shell model results.

The normal displacements of the nodes belonging to any given nodal layer are tied to a common, but otherwise free, value; those normal displacements constitute the residual unknowns of the stress recovery submodel.

It worth noting that, according to this modelling technique, the submodel normal displacements are fully detached from their counterpart along the underlying shell element, thus, e.g. precluding the application of transverse shear loads to the submodel. A possible future development consists in enforcing that the lateral edge nodes follow in (weighted) average the normal displacements of the underlying shell element nodes; the determining of appropriate weights appears to be, however, a far from being straightforward task.

The C1, C2, etc. mid-edge nodes displacement components are tied to the average value of their counterparts at the associated (B1,B2), (B2,B3), etc. pairs of lateral edge nodes.

The ILTS distribution returned by the stress-recovery submodel fed with the nodal motion of a quadrilateral shell element in correspondence of Fig. 1 point D, is reported with a dashed curve in Fig. 6, for a direct comparison with the control model results, reported as a solid line.

Although a 20% ILTS deviation from control values is observed, the results obtained thought the stress-recovery submodel correctly grasp the reference ILTS distribution trend, at a fraction of the computational effort.

4. Conclusions

A test was conducted on a geometry with a single curvature, revealing a complex induced trend of Inter-Laminar Tensile Strength (ILTS) throughout the thickness. The ILTS trend calculated using the 3D solid control model exhibits a nontrivial S-shaped through-the-thickness evolution, with both a compressive and a tensile peak. A basic analytical model from literature, see (Roos et al. 2007 b), is found to fall short in accurately reproducing this particular trend, due to an unsatisfied assumption regarding the role of in-plane shear strains.

A novel, local 3d solid submodel has been developed for ILTS retrieval from the displacement/rotation fields returned by a four-noded shell element representation of the structure under scrutiny; such stress retrieval submodel is processed through a standard finite element solver, and its results are aligned with those of the control model, within a 20% error band.

References

Daniel, P. M., Främby, J., Fagerström, M., Maimí, P., 2020. Complete transverse stress recovery model for linear shell elements in arbitrarily curved laminates. Composite Structures 252, 112675.

Dassault System, 2006. Abaqus 6.6 Analysis Users's Manual. Abaqus Theory Manual

Huang, N. N., Tauchert, T. R., 1992. Thermal stresses in doubly-curved cross-ply laminates. International Journal of Solids and Structures 29, 991–1000.

Irons, B. M. R., 1976. *'The semi-loof shell elements' in Finite Element for Thin Shells and Curved Membranes*. Eds. D. G. Ashwell and R. H. Gallagher

Kress, G., Roos, R., Barbezat, M., Dransfeld, C., Ermanni, P., 2005. Model for interlaminar normal stress in singly curved laminates. Composite Structures 69, 458–469.

Mao, K. M., Sun, C. T., 1991. A refined global-local finite element analysis method. International Journal for Numerical Methods in Engineering 32, 29–43.

MSC Software Corporation, 2013a. *Marc 2013.1 User Documentation, Volume A: Theory and User Information*. MSC Software Corporation

MSC Software Corporation, 2013b. *Marc 2013.1 User Documentation, Volume B: Element Library*

Pagano, N. J., 1970. Exact solutions for rectangular bidirectional composites and sandwich plates. Journal of composite materials 4, 20–34.

Rolfes, R., Rohwer, K., 1997. Improved transverse shear stresses in composite finite elements based on first order shear deformation theory. International Journal for Numerical Methods in Engineering 40, 51–60.

Rolfes, R., Noor, A. K., Sparr, H., 1998. Evaluation of transverse thermal stresses in composite plates based on first-order shear deformation theory. Computer Methods in Applied Mechanics and Engineering 167, 355–368.

Rolfes, R., Rohwer, K., 2000. Integrated thermal and mechanical analysis of composite plates and shells. Composites science and technology 60, 2097–2106.

Roos, R., Kress, G., Ermanni, P., 2007b. A post-processing method for interlaminar normal stresses in doubly curved laminates. Composite Structures 81, 463–470.